Research Repository UCD

Title	Grid-Forming Dynamic Stability under Large Fault Events – Application to 100% Inverter-based Irish Power System
Authors(s)	Zhao, Xianxian, Flynn, Damian
Publication date	2023
Publication information	Zhao, Xianxian, and Damian Flynn. "Grid-Forming Dynamic Stability under Large Fault Events – Application to 100% Inverter-Based Irish Power System." Taylor & Francis, 2023. https://doi.org/10.1201/9781003302520.
Publisher	Taylor & Francis
Item record/more information	http://hdl.handle.net/10197/13109
Publisher's statement	Set text: This is an Accepted Manuscript of a book chapter published by Routledge/CRC Press in Grid-Forming Power Inverters: Control and Applications on [date of publication], available online: http://www.routledge.com/9781003302520
Publisher's version (DOI)	https://doi.org/10.1201/9781003302520

Downloaded 2026-05-01 23:35:19

The UCD community has made this article openly available. Please share how this access benefits you. Your story matters! (@ucd_oa)

© Some rights reserved. For more information

EXAMPLE CHAPTER – Contributed chapter

Chapter 9: Grid-Forming Dynamic Stability under Large Fault Events – Application to 100% Inverter-based Irish Power System

Author(s):
*Xianxian Zhao (University College Dublin, xianxian.zhao@ucd.ie)
Damian Flynn (University College Dublin, damian.flynn@ucd.ie)

9.1 Grid-Forming Requirements for Future Grids with High Shares of Renewables

For many relatively small and synchronously isolated power systems, such as Ireland and Great Britain, to achieve net-zero ambitions, the integration of high shares of inverter-based renewable energy sources (mainly wind and solar photovoltaic) is necessary. Maintaining such power systems at a (near) constant frequency and voltage, while ensuring high reliability levels is particularly challenging, since, amongst various reasons, the increased variability and uncertainty associated with wind and solar generation, can lead to more frequent and larger voltage fluctuations, and challenges to generation-demand balancing.

The stability characteristics of synchronous generator-based power systems are well known and understood, since they are constrained by the physical electro-mechanical properties of such machines. However, power systems with high inverter shares can introduce new issues of concern. Figure 9.1 presents some major challenges associated with high renewable systems, while indicating the ease with which they can be potentially addressed. The challenges are mainly due to 1) device models being hidden, and the resulting power system dynamic characteristics not being clearly defined, and 2) analysis methods to assess device and system behaviours still being in development [1][2]. Clearly, it follows that more detailed (and open) models are required, supported by enhanced device control methods, and more advanced stability assessment tools, including recognition of new phenomena, such as inverter control interactions [3].

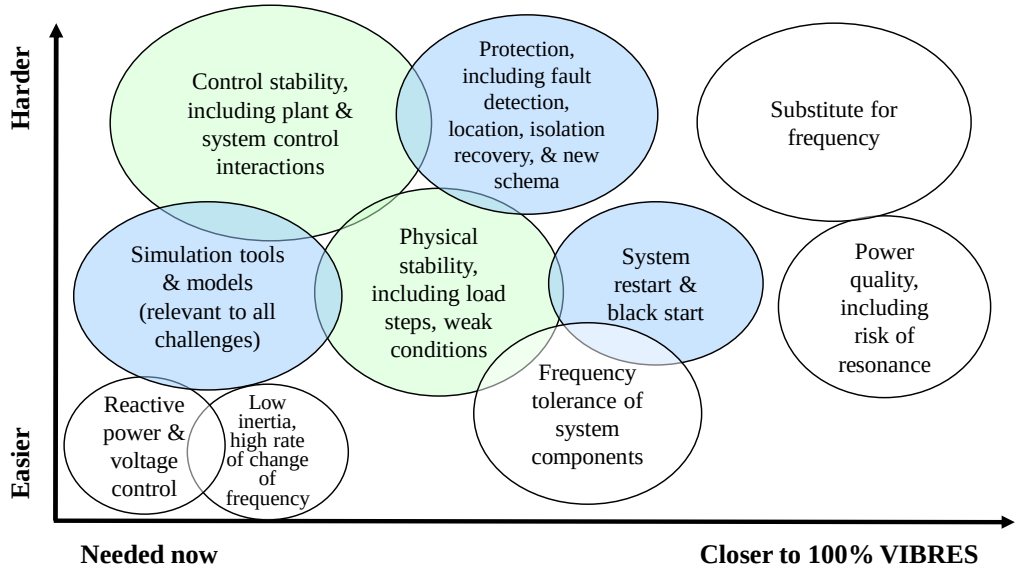

Figure 1: Stability challenges associated with achieving higher shares of inverter-based renewable energy sources [4].

At present, power electronic inverters, as typically seen in wind and PV farms, are mostly grid-following in nature, such that they follow the grid voltage angle using phase-locked loops (PLLs), and they behave as current sources. Hence, grid-following inverters cannot operate without synchronous machines (SGs), or synchronous condensers (SCs) nearby, since they need something to follow, and they require relatively stiff grids (rates of change of system states should be much slower than the PLL response speed) in order to achieve their control targets. However, with few or no SGs (or SCs) online nearby, the system states are likely to vary much more dynamically, and individual inverter PLLs may struggle to satisfactorily achieve the required tracking capability. This is particularly true for grid-following inverters connected at weak grid locations, leading to reduced transient performance and increased likelihood of system instability [5]. Therefore, grid-forming inverters (GFMIs), which are able to independently create the grid voltage frequency and angle without relying on nearby SGs or SCs, and which can provide an immediate response to system disturbances by behaving as voltage sources, are anticipated to offer a technical and economical solution towards

maintaining the same reliability standards and stability levels as today [6]. It is noted that GFMIs are distinct from grid-supporting inverters, with the latter also being able to support the grid voltage and frequency, but they require nearby GFMIs, or SGs, since they don't independently generate their own voltage angle but instead employ PLLs to synchronise themselves with the grid. Consequently, they can also be categorised as being grid-following inverters.

As grid-forming inverters are envisioned to replace synchronous machines, many different grid-forming controls have been proposed, mainly divided as: droop control [7][8][9], mimicking synchronous machine operation by emulating a synchronous machine's physical dynamics [10], or reproducing the swing equation [11][12], synchronous machine matching control using the DC-link capacitor voltage to realise the swing equation [13][14][15], and virtual oscillator control [16][17]. Grid-forming pilot projects and field demonstrations are also emerging, most notably for battery energy storage systems [18] and wind turbines [19]. Given the likely increased importance of grid-forming inverters for future systems, and particularly noting decarbonisation aspirations in many countries, it follows that power systems entirely based on power electronics inverters (wind, solar, battery, HVDC interconnection) may not be that far away. Consequently, GFMI dynamic stability under large fault events is of interest, and a reduced Irish transmission grid with 100% power electronic inverters, without any synchronous machines, is considered as a test case. In comparison to synchronous generators, GFMIs exhibit much superior voltage and frequency regulation capability, if the energy input and inverter overcurrent capability are assumed ideal, due to the fast and full controllability of voltage source inverters [8][10]. However, for fault events, the limited overcurrent capability (2~3 times smaller than SGs) of GFMIs is an issue, and instability problems can result if the current limiting control is not suitably designed [20]. The dynamic stability of GFMIs under "hard" current reference (with [21], or without [22][23], anti-windup integration for the outer

voltage loop, using active current prioritisation [22], or scaling current approach [21][23]), "soft" virtual impedance (VI) current limiting [24], or an intricate projected method (where the real-time grid short-circuit ratio needs to be estimated [25]) has been extensively studied for balanced faults. A "soft" virtual impedance current limiter is required for GFMIs, since it not only makes the inverter more robust for both fault and downward phase jump disturbances, as compared to "hard" direct current reference limiting, but also avoids high-frequency oscillations, which can be easily excited by active or reactive current prioritisation current reference limiting (shown later in the chapter). Under both fault and grid phase jump events, while ensuring strict current limiting, a combination of both hard and soft current limiting measures has also been proposed for GFMIs to aid their transient stability [27]. Moreover, virtual angular speed freezing has been proposed for GFMIs, in order to enhance transient stability under fault conditions. Given that wind and solar farms will most likely be in different locations to existing synchronous machines, the rating and location of GFMIs have been shown to be critical to securely operating the grid in the presence of both grid-forming and grid-following inverters [28][29], while distributing grid-forming inverters at individual buses across the system can reduce GFMI requirements [30][31]. However, although GFMI transient stability under fault conditions has been extensively studied, case studies based on real systems and associated validations remain few.

The remainder of the chapter is organised as follows: droop, virtual synchronous machine and dispatchable virtual oscillator (dVOC) control for grid-forming inverters are introduced, supported by current reference and virtual impedance (VI) current limiting control, and virtual angular speed freezing, in Section 9.2; *Urban* and *Remote* scenarios for inverter locations for a future Irish transmission system are considered in Section 9.3, and an array of case studies are presented, including the *Urban* Irish grid with 100% GFMIs (all droop (or virtual synchronous machine) control, all dVOC control, or a mix of both), with hybrid current

limiting and without virtual angular speed freezing control, and case studies of the *Remote* Irish grid with 100% GFMIs under either current reference or VI current limiting control, and with/without virtual angular speed freezing; finally, Section 9.4 draws conclusions for operating and controlling 100% power electronic based power systems.

9.2 Grid-Forming Inverter Modelling, Current Limiting and Control Design

Droop, VSM and dVOC control-based GFMIs, with inner cascaded voltage and current proportional integral (PI) control, together with a number of current limiting control schemes (active and reactive priority, scaled current reference and virtual impedance current limiting) are introduced, while a virtual angular speed freezing technique is presented to enhance transient stability, while being insensitive to phase jumps. Synchronous machine matching control using the DC-link capacitor voltage to realise the swing equation [13][14][15] has been shown to cause large deviations in the DC-link voltage (which needs to be tightly controlled, notably for HVDC and wind turbine applications), and hence is not studied here.

9.2.1 Droop control with inner cascaded voltage and current PI control loops

A voltage source inverter with a PI-controlled DC current source, capacitor and LCL filter is shown in Figure 9.2 connected to an AC grid. The DC current source represents the DC-side input power, perhaps from a PV panel, wind turbine or energy storage system. The AC grid is represented by an ideal voltage source in series with an impedance (R_g, L_g), while a step-up transformer, R_c, L_c, represents the grid-side RL filter. Figure 9.2 also indicates a droop-based control structure, with cascaded voltage and current PI decoupling control loops. The active power/frequency droop control generates the inverter internal voltage angular speed, ω_{vsm}, and angle, θ_{vsm}. The reactive power/voltage droop control generates the voltage deviation, ΔV, which is then combined with V^* to form the d-axis output voltage reference, v_{od}^*. The q-axis

output voltage reference, v_{oq}^{*}, is set to zero, such that the dq frame for the decoupling control rotates at speed ω_{vsm}, with the d-axis aligned to the internal / output voltage across the LCL filter capacitor. A cascaded voltage and current PI control structure has been adopted here, since the LC filter dynamics can be fully exploited to achieve the GFMI control requirements and current limiting. The PI controller parameters are based on [32], which are tuned to provide the largest damping ratio for a grid-forming inverter connected to a grid with a high short-circuit ratio. Damping enhancement control (Δe_d and Δe_q are the high-pass filter output of the output current i_{od} and i_{oq}) is also incorporated to the output voltage references, v_{od}^{*} and v_{oq}^{*}.

Threshold virtual impedance current limiting is also shown in Figure 9.2, whereby if the measured inverter current magnitude, I_c, exceeds the specified value, I_{nom}, the virtual resistance and reactance, $R_{VI} > 0$ and $X_{VI} > 0$, and the VI control are activated. The generated dq axis voltage drops, ΔV_{VId} and ΔV_{VIq}, are then combined with v_{od}^{*} and v_{oq}^{*}. The VI control parameters (kp_R^{VI} and $\sigma_{X/R}^{VI}$) are tuned to limit the inverter current to I_{max}^{VI} when a bolted three-phase fault is applied at the capacitor filter terminals, based on the tuning principles described in [24].

The control logic for the scaled current reference limiting control is shown in Figure 9.3, such that when $I_c^{*0} \geq I_{max}^{sat}$, i_{cd}^{*0} and i_{cq}^{*0} are scaled to ensure that $i_{cd}^{*2} + i_{cq}^{*2} \leq I_{max}^{2}$, while, the integrator of the outer PI controller is frozen by setting its input to zero. Figure 9.3 also shows the active current (d-axis) prioritised current reference limiting, while reactive current (q-axis) prioritised limiting is the same as its active current counterpart with d and q subscripts exchanged (further details in [26][33]). It is noted that alternative strategies can achieve the same mathematical relationship, $\sqrt{i_{cd}^{*2} + i_{cq}^{*2}} \leq I_{max}^{2}$, for example, $i_{cd}^{*} = I_{max}\cos(\theta)$, $i_{cq}^{*} = I_{max}\sin(\theta)$, where θ is a fixed angle, as in [34].

If only current reference limiting control is applied it is likely that the GFMI in Figure

9.2 will quickly lose stability or output high-frequency power oscillations following a large fault disturbance or downward phase jump (GFMI stability under upward phase jumps is of little concern [27]). Inverter stability can be improved if "soft" VI current limiting control is incorporated, since when virtual impedance is activated, the outer voltage PI control operates as normal, and the output voltage can be directly controlled. However, the initial inverter fault current can still be high, with a decay time of ≈20 ms. Consequently, a combination of VI and scaled current reference saturation control is proposed. In comparison with the current reference saturation strategy implemented in [34], scaling acts in proportion to the current magnitude, such that it is not necessary to define a fixed current reference angle. The current limit for current saturation control is set higher than that for VI control, $I_{max}^{VI} < I_{max}$, for example, 1.25 pu relative to 1.2 pu. Thus, scaled current reference control tends to be active during the initial transients, while VI control dominates the "longer term" GFMI dynamics.

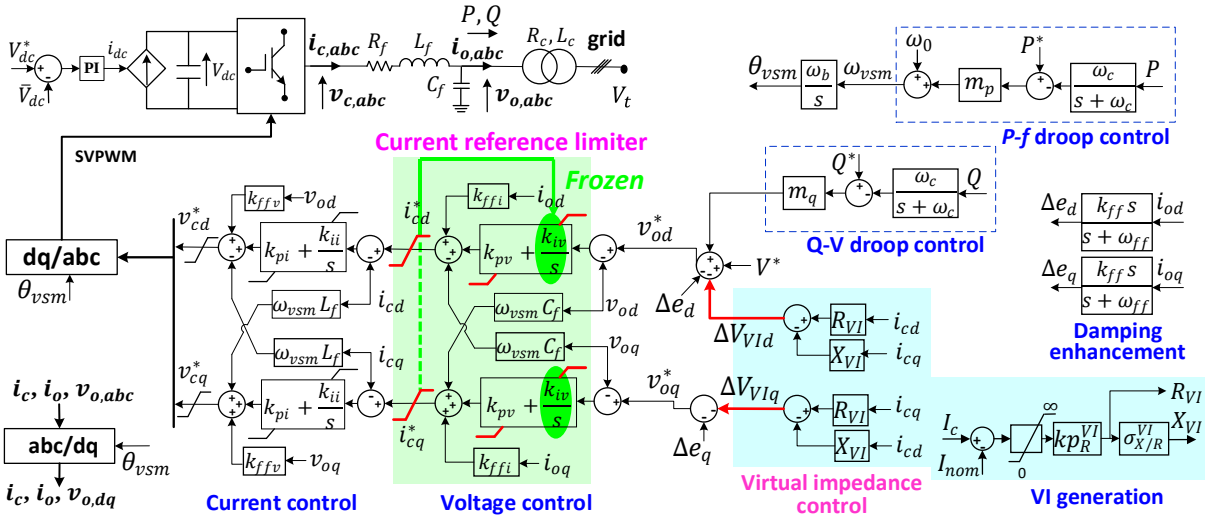

Parameter	Value (pu)	Parameter	Value (pu)
R_f, L_f, C_f,R_c, L_c	0.005, 0.15, 0.066, 0.005, 0.15	C_{dc}, K_p^{dc}, K_i^{dc}	2 mF, 82, 2048
m_p, m_q	0.02, 0.0001	$(i_{cd}^{*2} + i_{cq}^{*2})^{0.5} \le I_{max}$	$I_{max} = 1.25$ *or* $1.1\ pu$
K_{ffi}, K_{ffv}, ω_{ff}, K_{ff}	1, 1, 16.66, 0.01	kp_R^{VI}, I_{max}^{VI}	$0.67, 1.2\ pu$
V_{dc}^*, V^*, Q^*, ω_0	1, 1, 0, 1	Or kp_R^{VI}, I_{max}^{VI}	$1.49, 1.1\ pu$
k_{pv}, k_{iv}, k_{pi}, k_{ii}	0.52, 1.161022, 0.7388, 1.19	$\sigma_{X/R}^{VI}$, I_{nom}	$5, 1\ pu$

Figure 9.2: Grid-forming inverter connected to a DC current source and an AC grid via a LCL filter under droop-based control, with a combination of virtual impedance and saturation current limiting, and a damping enhancement block, and its control structure and parameters.

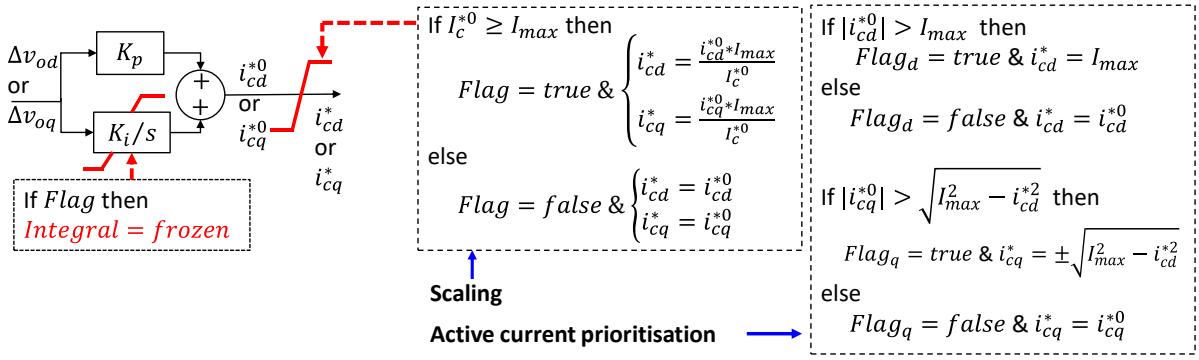

Figure 9.3: Current scaling and active current prioritisation saturation limiter including anti-windup integration in outer voltage PI control, where i_{cd}^{*0} and i_{cq}^{*0} are the d- and q-axis current references from the outer voltage control loop, and I_c^{*0} is the relevant amplitude.

9.2.2 Virtual synchronous machine control

Virtual synchronous machines (VSM), also known as virtual synchronous generators (VSG), or synchronverters, have been widely studied. A synchronverter [10] emulates the electrical behaviour of a synchronous machine, while a VSM [11][12] reproduces the swing equation to generate the voltage reference, as shown in Figure 9.4(a). However, a fixed $\omega_0 = 1$ pu is applied here, instead of an estimated frequency from a phase-locked-loop, as in [11], noting that a grid-forming inverter should independently form the grid voltage angle and avoid fundamental shortcomings of grid-following inverters. Figure 9.4(a) matches Figure 9.4(b), since the former can be formulated and transformed as

$$\omega_{vsm} = \frac{1}{2Hs}\left(P^* - P - K(\omega_{vsm} - \omega_0)\right), \tag{9.1}$$

$$(2Hs + K)\omega_{vsm} = P^* - P - K * \omega_0, \tag{9.2}$$

$$\omega_{vsm} = \frac{P^* - P}{2Hs + K} - \frac{K}{2Hs + K}\omega_0 = \frac{P^* - P}{2Hs + K} - \omega_0, \tag{9.3}$$

Equation (9.3) is shown in Figure 9.4(b), such that Figure 9.4(a)(b) are equivalent.

The VSM control in Figure 9.4(a)(b) is the same as the P/f droop control in Figure 9.2, which can be expressed and transformed as follows

$$\omega_{vsm} = m_p \left(P^* - \frac{\omega_c}{s+\omega_c} P \right) + \omega_0, \tag{9.4}$$

$$\omega_{vsm} = m_p \left(\frac{\omega_c}{s+\omega_c} (P^* - P) \right) + \omega_0 = \frac{1}{\frac{1}{m_p \omega_c} s + \frac{1}{m_p}} (P^* - P) + \omega_0. \tag{9.5}$$

Therefore, the form of (9.3) and (9.5) are equivalent, noting that

$$H = \frac{1}{2 m_p \omega_c}, \qquad K = \frac{1}{m_p}. \tag{9.6}$$

As will be shown later in Section 9.3, the VSM and droop controls create the same simulation results, subject to the parameter selections defined in (9.6), and other control aspects being unchanged. When designing a robust droop control implementation, a large number of simulation studies suggests that the droop coefficient should be selected as $m_p \leq 0.02$ [32]. A low value for m_p implies a strong load sharing contribution for a grid-forming inverter, while recognising that $m_p = 0.04$ or 0.05 is typical for thermal (synchronous machine) power plants. With m_p (or damping coefficient K) chosen, ω_c (or H) must also be selected. Small H improves small-signal stability, or small-disturbance oscillatory stability, with power oscillations quickly damped. In contrast, for large H, more "inertial" energy is stored, and the (virtual) rotor speed will deviate more slowly under large disturbances, such as severe faults, generator trips, etc.

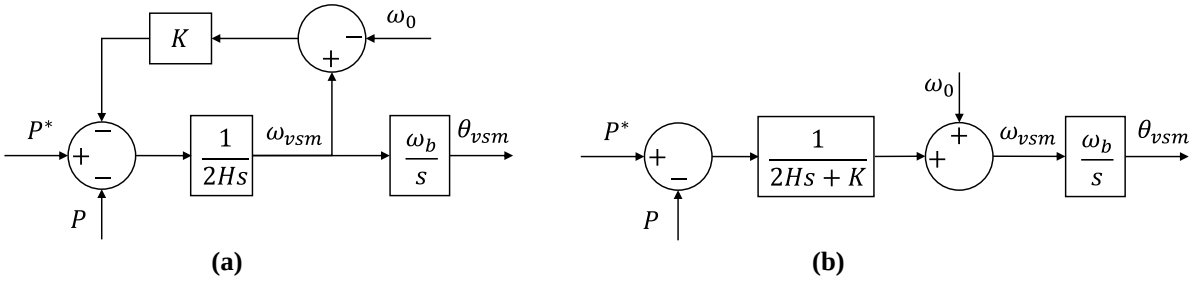

Figure 9.4: Virtual synchronous machine control, (a) is equivalent to (b).

9.2.3 Dispatchable virtual oscillator control-based grid-forming inverter modelling

Dispatchable virtual oscillator (dVOC) control adopts a different approach to generating the voltage amplitude and angle references, by recognising the couplings between active and

reactive power [17]. Both droop (or VSM) and dVOC controls are investigated under fault conditions in Section 9.3. The implemented dVOC control strategy follows the same principles as those shown in Figure 9.2, except that the virtual angle, θ_{vsm}, and dq-axis voltage references, v_{od}^* and v_{oq}^*, are generated as

$$\frac{1}{\omega_b}\begin{bmatrix}\dot{u}_{o\alpha}^*\\ \dot{u}_{o\beta}^*\end{bmatrix} = \eta\left(K\begin{bmatrix}u_{o\alpha}^*\\ u_{o\beta}^*\end{bmatrix} - R(\rho)\begin{bmatrix}i_{o\alpha}\\ i_{o\beta}\end{bmatrix} + \alpha\left(1-\frac{U_o^{*2}}{V_{ref}^2}\right)\begin{bmatrix}u_{o\alpha}^*\\ u_{o\beta}^*\end{bmatrix}\right),$$

$$K = \frac{1}{V_{ref}^2}R(\rho)\begin{bmatrix}P_{ref} & Q_{ref}\\ -Q_{ref} & P_{ref}\end{bmatrix}, \tag{9.7}$$

$$\theta_{vsm} = \omega_0 t + \tan^{-1}\left(\frac{u_{o\beta}^*}{u_{o\alpha}^*}\right), \qquad \omega_{vsm} = \dot{\theta}_{vsm}/\omega_b, \tag{9.8}$$

$$v_{od}^* = \sqrt{u_{o\alpha}^{*2} + u_{o\beta}^{*2}} - \Delta V_{VId} - \Delta e_d, \quad v_{oq}^* = 0 - \Delta V_{VIq} - \Delta e_q, \tag{9.9}$$

where, $R(\rho_i) = \begin{bmatrix}\cos(\rho_i) & -\sin(\rho_i)\\ \sin(\rho_i) & \cos(\rho_i)\end{bmatrix}$, $\rho_i = \frac{l_i}{r_i}$, and l_i and r_i are the transmission line inductance and resistance. Here, ρ_i is assumed to be the same for all transmission lines (in [35], simulation and experimental results both demonstrate that the system remains stable even when this assumption is not true). In order to achieve a fair comparison, the "soft" virtual impedance current limit and damping enhancement controls shown in Figure 9.2 are also applied to v_{od}^* and v_{oq}^* in (9.3). Details of the dVOC controls are shown in Figure 9.5, with $\eta/V_{ref}^2 = m_p$, $\alpha V_{ref} = 1/m_q$, such that the dVOC steady-state active and reactive power droop settings are equivalent to the previous droop control settings (whose steady-state droop characteristic can be found in [36]). In addition, for the case studies shown in Section 9.3, the voltage setpoints, and active and reactive power setpoints for both controls are unchanged.

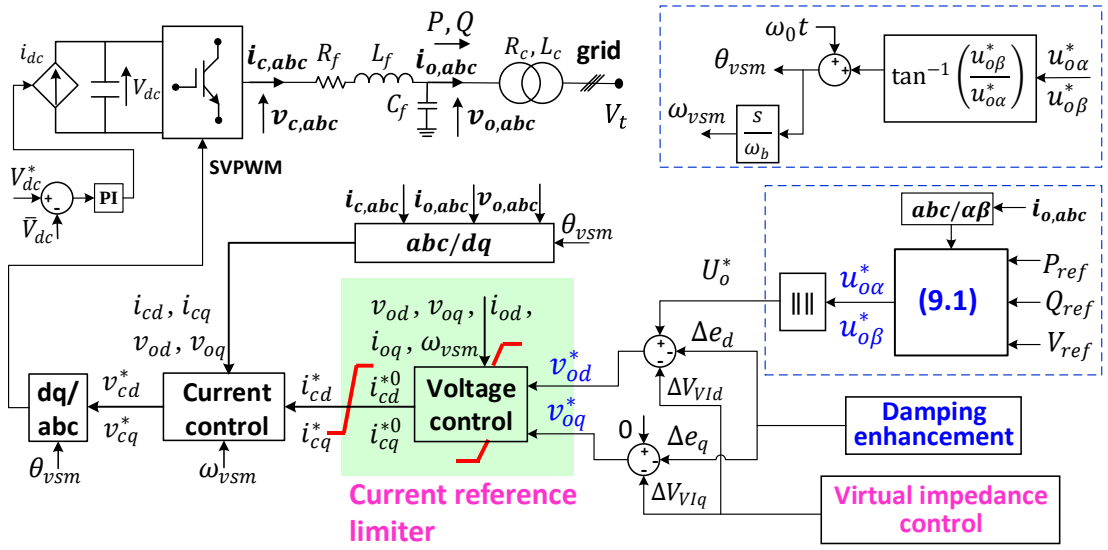

Figure 9.5: Grid-forming inverter under dispatchable virtual oscillator control, combined with virtual impedance and current saturation limiters, and a damping enhancement block.

9.2.4 Grid-forming inverter angular speed freezing

The transient stability of grid-forming inverters is affected by the transient evolution of the voltage angle, and the d- and q-axis components of the generated voltage. Since a power system may consist of many grid-forming inverters, each employing different control strategies, and utilising different parameters, analysis of such systems can be challenging. Here, instead of controlling the virtual angular speed, or the associated angle, for each GFMI, it is proposed that their virtual angular speeds are frozen to their pre-fault values when a fault is detected and the inverter current exceeds a certain value (see Figure 9.6). It follows that the relative angular differences between the GFMIs after a fault is cleared should be relatively similar to the pre-fault values (variations will occur due to specific system conditions and parameter settings). Considering the power-angle relationship and equal area criterion, if the relative angle between voltage sources doesn't change too much during a fault, then the system is more likely to remain stable, and since all the GFMIs are frozen to the same angular speed it follows that the fault critical clearing time should be increased. The freezing action is activated when both the

output voltage and active power (V and P) are lower than the defined thresholds, V_l and P_l. Including the active power, P, input avoids the freezing action being triggered during grid phase jump down events. Finally, it is noted that no communication is required to implement the freezing technique, as seen in Figure 9.6, but the frozen angular speed input can be updated, as required, as system conditions change, using (slow) communications, or otherwise.

The virtual angular speed freezing technique of Figure 9.6 is formulated as (9.10)

$$\omega_{vsm} = \begin{cases} normal, & \text{Otherwise} \\ \omega_{vsm}^{0}, & \text{fault \& } (\mathrm{I_c} > \mathrm{I_{nom}}) \text{ or fault \& } (\mathrm{I_c^{*0}} > \mathrm{I_{max}} - \Delta \mathrm{I}) \end{cases} \tag{9.10}$$

where, if only current reference saturation limiting is used, the logic $\mathrm{I_c^{*0}} > \mathrm{I_{max}} - \Delta \mathrm{I}$ is chosen, otherwise $\mathrm{I_c} > \mathrm{I_{nom}}$ (i.e. virtual impedance is activated).

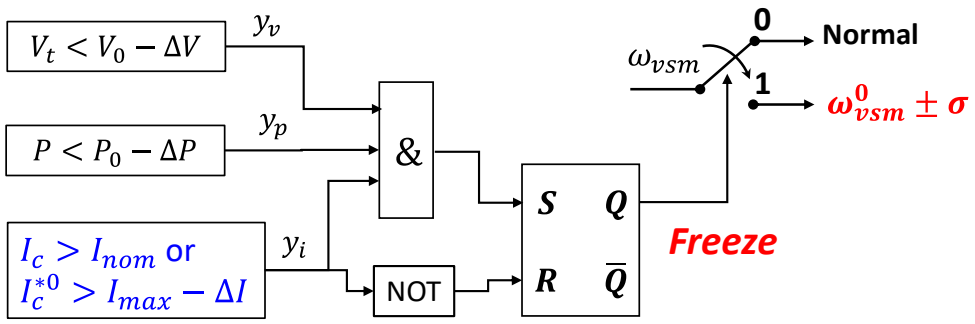

Figure 9.6: Unified virtual angular speed freezing for a grid-forming inverter system without synchronous generators (condensers), where V_0, P_0 and ω_{vsm}^0 are the pre-fault terminal voltage, active power output and virtual angular speed, and ΔV, ΔP and ΔI are small constants, set here as 0.25, 0.2 and 0.05 pu. σ is a small positive constant, giving the GFMI additional freedom (e.g. small negative σ can speed up GFMI post-fault recovery for $P_0 > 0$ and very weak connections), and set as 0 here.

9.3 Irish Grid Case Study With 100% Grid-Forming Inverters

The transient dynamics of a reduced Irish transmission system based on the 2015 Irish winter peak demand with all generation being based on grid-forming inverters is considered, in order

to assess some of the stability issues associated with future 100% renewable (wind and solar) power systems. For the test system, individual grid-forming inverters can either employ droop (or VSM) control or dVOC control, with options for VI and scaled current reference saturation control, and virtual angular speed freezing also considered. Electromagnetic transient (EMT) simulations are performed under the Dymola environment using the Modelica modelling language [37], whereby all modelling details are completely transparent and user-created models can be easily integrated. The focus here is placed on the transient stability impact of replacing synchronous generators by grid-forming inverters on a test system, but relevant theoretical analysis on single-machine infinite bus system has been considered elsewhere [27][38].

9.3.1 Urban and Remote grid models

The Ireland and Northern Ireland transmission system is synchronously isolated from Great Britain and the rest of the European continental system, with operating voltage levels of 400, 275, 220 and 110 kV [39]. Most of the conventional generating fleet is connected at 220 kV and above voltage levels, although the majority of the network consists of 110 kV circuits spread across the entire system. Ireland is targeting up to 80% renewable generation by 2030, which implies that for ≈50% of the time, wind and solar availability will exceed the instantaneous demand [40]. However, due to system stability and security concerns, a system non-synchronous penetration (SNSP) upper limit of 75% is currently imposed, which is defined as follows:

$$SNSP = \frac{P_W + P_{HVDC(imp)}}{P_L + P_{HVDC(exp)}} \tag{9.11}$$

where, P_W, P_L, $P_{HVDC(imp)}$ and $P_{HVDC(exp)}$ are the actual wind (and solar) power, load demand, and power imported/exported through HVDC links, respectively. The system operators, EirGrid and SONI, have proposed pushing the SNSP ceiling towards 95% and beyond [40],

but for a variety of technical reasons, operating the system at 100% SNSP is not yet considered viable, even if the instantaneous wind (and solar PV) share at any point in time could enable this to be achieved. Consequently, the Irish grid, which is synchronously isolated, and already accepting high SNSP levels, can be considered as a good starting point for investigating plausible 100% inverter-based systems without excessive network and/or load/generation growth changes being required. However, the operational rules for a 100% inverter based system are likely to be noticeably different.

For systems with high inverter shares, particular focus must be placed on network faults, given the limited overcurrent capability of inverters, while also noting that they tend to be 2~3 orders of magnitude smaller in power rating relative to synchronous generators. Since three-phase faults generally represent a worst case scenario, they are considered here for a 100% inverter-based Irish grid.

Figure 9.7(a) shows the reduced *Urban* Irish transmission grid, with important aspects of the simulation setup summarised:

- Only the 400, 275 and 220 kV transmission system voltage levels are represented, with lower voltage levels represented by equivalent loads. In total, 82 bus nodes, 47 constant impedance loads (actual and equivalent), 14 inverters, 110 transmission lines (equivalent π model), and multiple shunt capacitors and transformers are included.
- The 2015 Irish winter peak demand is applied, with ≈6 GW and ≈1.3 GVAr of active and reactive loads, acknowledging relatively flat demand growth in Ireland in recent years.
- For the *Urban* configuration, the inverters are placed at the same locations as the critical set of on-line conventional units, based on existing operational (steady-state network loading and stability) rules for the Irish power system [41]. Such an approach implies that system-level issues, such as inter area flows, line overloading, voltage support, system reserves, etc., which may result due to changes in size and location of (renewable-based)

inverters displacing fossil-fired synchronous generators are largely avoided. Instead, focus is placed on the change (from synchronous machine to inverter) in the generation sources themselves.

- Individual inverter(s) are assumed to be large in size, with the same rating as the existing conventional units, in order to reduce the number of parameters being modified between the existing and 100% inverter-based systems.

Figure 9.7(b) presents the *Remote* grid configuration, whereby the inverters are placed in more remote parts of the network (and at lower voltage levels), as might be expected in a variable renewables-dominated system [42]. Additional 110 kV lines (not shown in Figure 9.7(b)) are included in the western parts of the system to connect the new inverters to the transmission network. Both grids possess the same inverter capacity and load demand, but, for the *Remote* system, additional capacitors are added, as necessary, at inverter buses in the east and west, to maintain system voltage levels within acceptable levels.

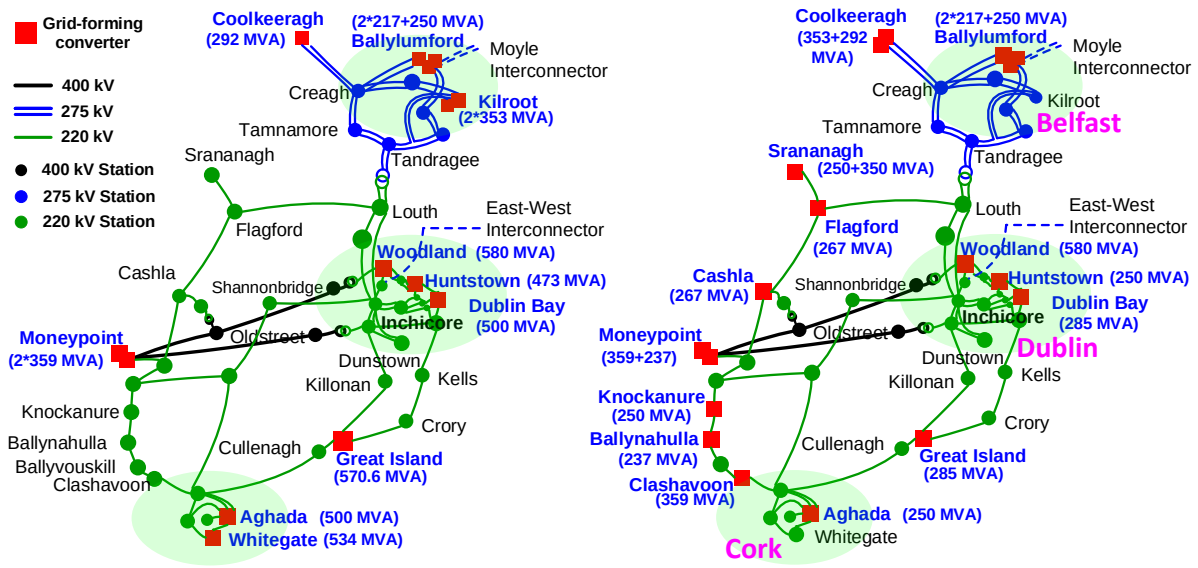

(a) (b)

Figure 9.7: Single line diagram of (a) *Urban* and (b) *Remote* Irish grids with 100% grid-forming inverters, with bus nodes roughly corresponding to geographical locations.

9.3.2 *Urban* Irish grid with 100% GFMIs (droop, dVOC control)

3-phase faults are applied at all buses of the reduced *Urban* Irish grid in Figure 9.7(a), assuming that all the inverters are grid-forming, and that they are operating under either droop control or virtual oscillator control. Three buses are selected to present the results: Woodland, Kilroot and Great Island, located near Dublin, Belfast, and the rural region between Dublin and Cork, respectively. These locations are chosen for two main reasons: proximity to the major load centres, and proximity to the inverter locations.

Initially it is assumed that all the grid-forming inverters are based on droop control, with the combination of virtual impedance and scaling current reference saturation control, and imposed current limits of 1.2 and 1.25 pu respectively. A 3-phase, 200 ms bolted fault is applied at the Woodland (near Dublin) bus. Figure 9.8(a) shows the voltages at the three selected buses, with the voltage at Woodland falling close to zero, since it is close to the fault location, while the voltage dips at the other two, more remote, buses are not as large, with Kilroot being further away than Great Island. After clearing the fault, the voltage recovers quickly at all the buses, and the oscillations dissipate after less than 20 ms. Figure 9.8(b)(c) shows the reactive (and active) power output immediately increasing (and reducing) after the fault occurs, with steady-state levels achieved within approximately 250 ms. The largest reduction in voltage is seen at the Woodland bus, given that it is closest to the fault location. Figure 9.8(d) shows the injected current from the inverters, which is limited in steady-state below the 1.2 pu limit (due to parameter tuning of the virtual impedance current limiting control), even for the Woodland inverter. However, the injected current initially exceeds 1.2 pu (but still less than 1.25 pu) when the fault occurs, with the current saturation control strictly limiting the current within 1.25 pu.

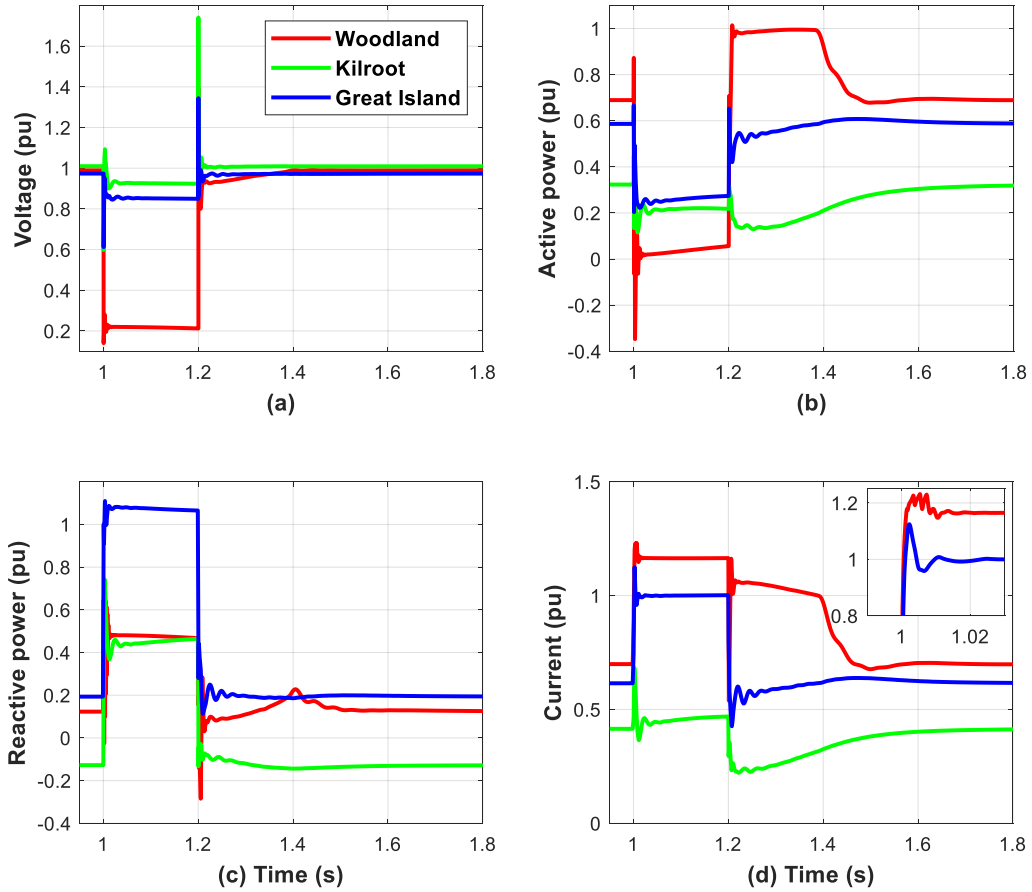

Figure 9.8: Voltage, active & reactive power output, and injected current of three GF inverters near Dublin, Belfast and Cork for a 200 ms, 3-phase bolted fault at the Woodland bus of the *Urban* Irish grid with 100% grid-forming inverters under droop control (combination of virtual impedance and current scaling limiting applied).

In order to confirm that the "hard" current saturation control, when combined with virtual impedance current limiting control, does not negatively impact on system stability, Figure 9.9 shows the case when only "soft" VI current limiting is implemented. The results in Figure 9.9(a)-(d) are very similar to those in Figure 9.8(a)-(d), except that the current for the Woodland inverter transiently exceeds 1.4 pu and oscillates for ~20 ms (confirming that the virtual impedance control response time is too slow to limit the initial current, which involves measuring the current before modifying the filter capacitor voltage references. The outer

voltage control loop slows the response). Given that similar system behaviour is achieved with/without current saturation control, the combined hybrid current limiting option is adopted for subsequent simulations of the *Urban* Irish grid.

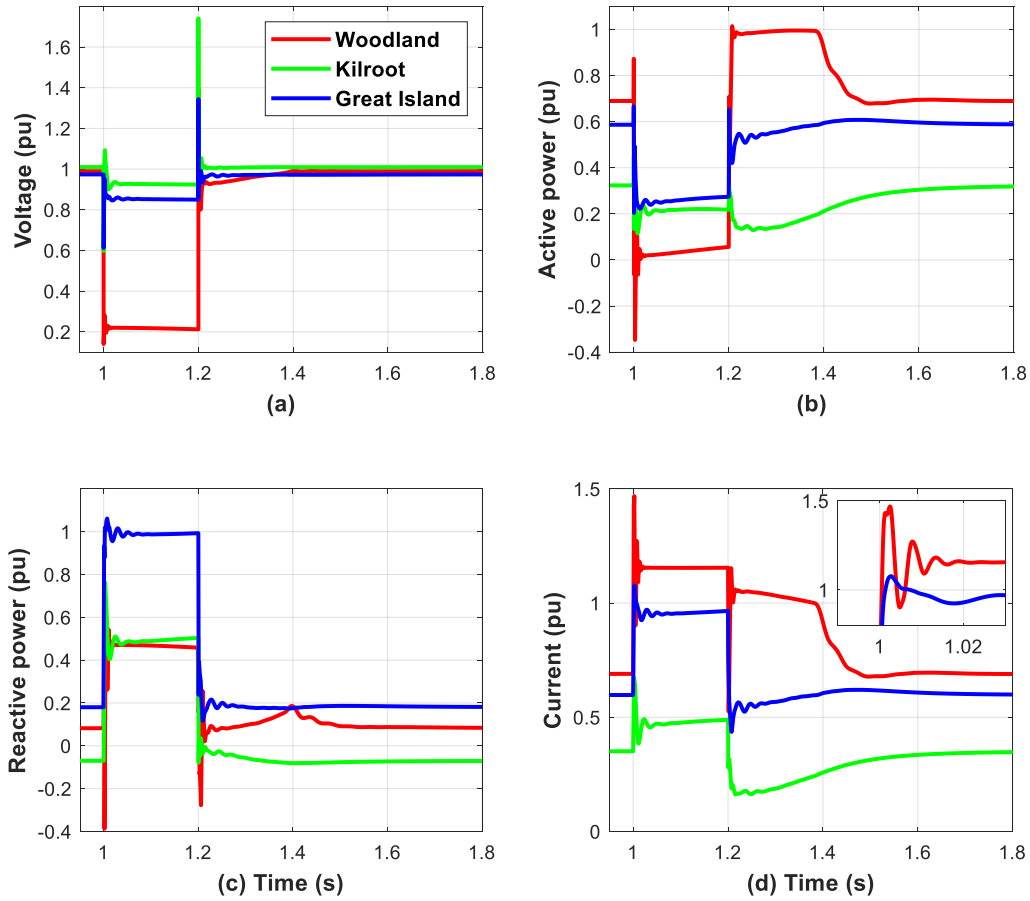

Figure 9.9: Voltage, active & reactive power output, and injected current of three GF inverters near Dublin, Belfast and Cork for a 200 ms, 3-phase bolted fault at the Woodland bus of the *Urban* Irish grid with 100% grid-forming inverters under droop control (virtual impedance current limit only applied).

The inverter control strategy is now switched from droop control to dispatchable virtual oscillator (dVOC) control, with the same fault conditions and fault location as above considered in Figure 9.10. The results are similar to Figure 9.8, mainly because: (a) for an inductive network, dVOC control resembles droop control [17], (b) the steady-state

expressions for the outer loop voltage references, and virtual angular speed and angle, are tuned to provide similar performance at nominal voltage, and (c) the same current limiting strategies are applied, which, when active, dominate the transient response. It follows that the nature of the current limiting strategies should form an important aspect of assessing the transient stability of grid-forming inverter based systems. In comparison with droop control, the dVOC approach achieves a faster recovery period, given that the frequency and voltage responses are directly coupled, which leads to a reduction in the virtual frequency deviation (as seen in Figure 9.11) and, a smaller increase in the virtual angle during the fault.

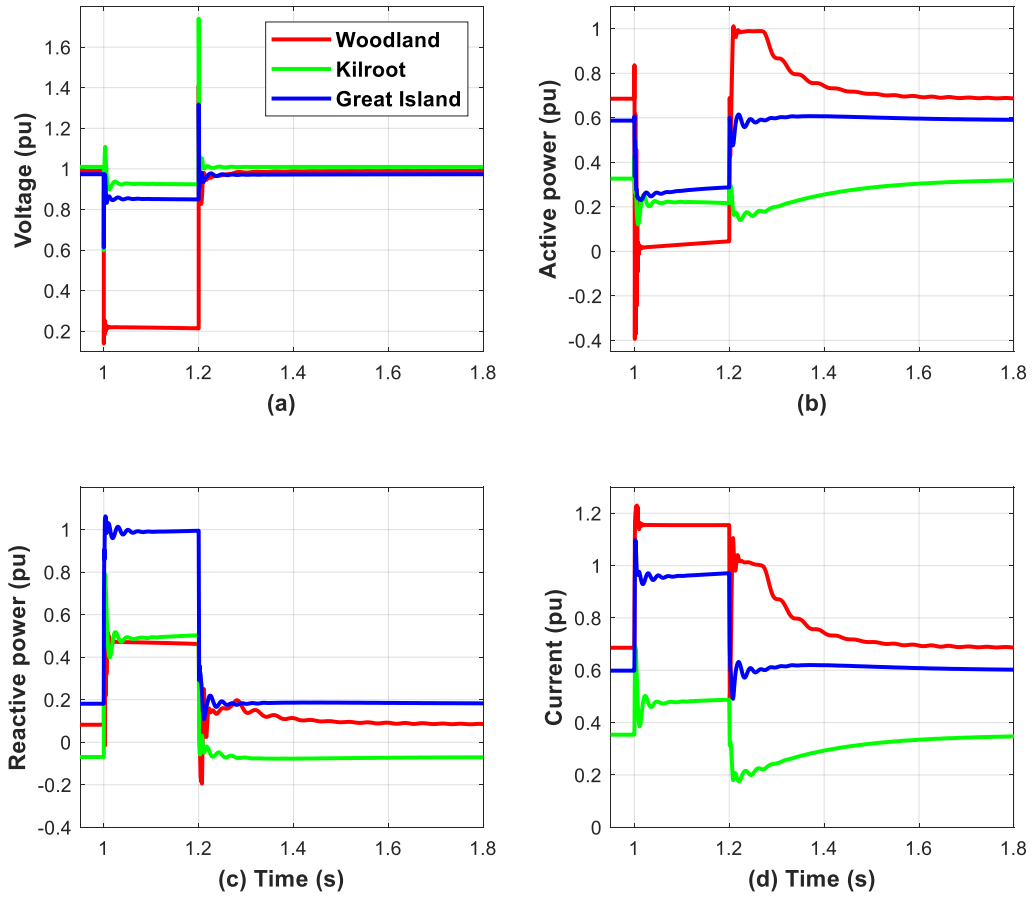

Figure 9.10: Voltage, active & reactive power output, and injected current of three GF inverters near Dublin, Belfast and Cork for a 200 ms, 3-phase bolted fault at the Woodland bus of the *Urban* Irish grid with 100% grid-forming inverters under dVOC control (combination of VI and saturation current limiting controls applied).

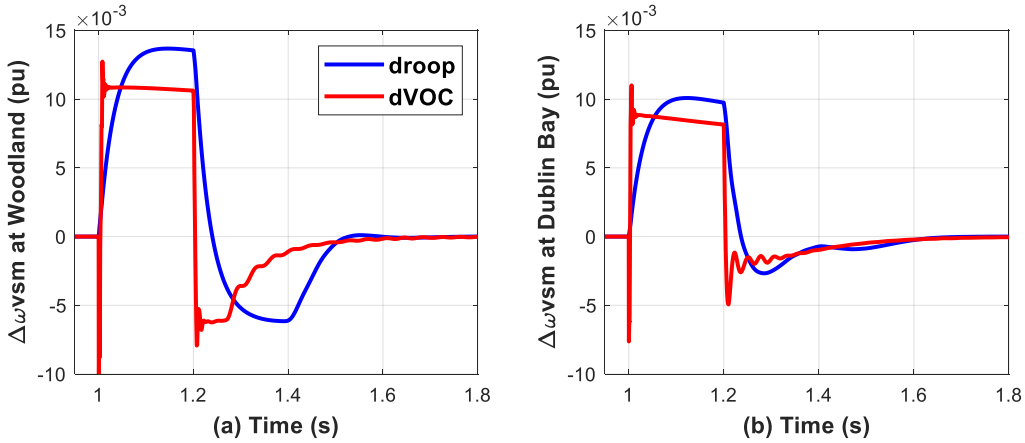

Figure 9.11: Virtual angular speed deviation, $\Delta\omega_{vsm}$, for two GF inverters at Woodland and Dublin Bay near Dublin for a 200 ms, 3-phase bolted fault at the Woodland bus of the *Urban* Irish grid with 100% grid-forming inverters under droop or dVOC control.

To confirm that the virtual synchronous machine (VSM) control in Figure 9.4 is the same as the droop control in Figure 9.2, VSM control is now applied for the same fault condition, with $H = 0.7962$ s and $K = 50$ in order to satisfy Equation 9.6. The simulation results are shown in Figure 9.12, with Figure 9.8 (droop control) superimposed. The similarity of the active power and injected current traces demonstrates that VSM control is equivalent to droop control.

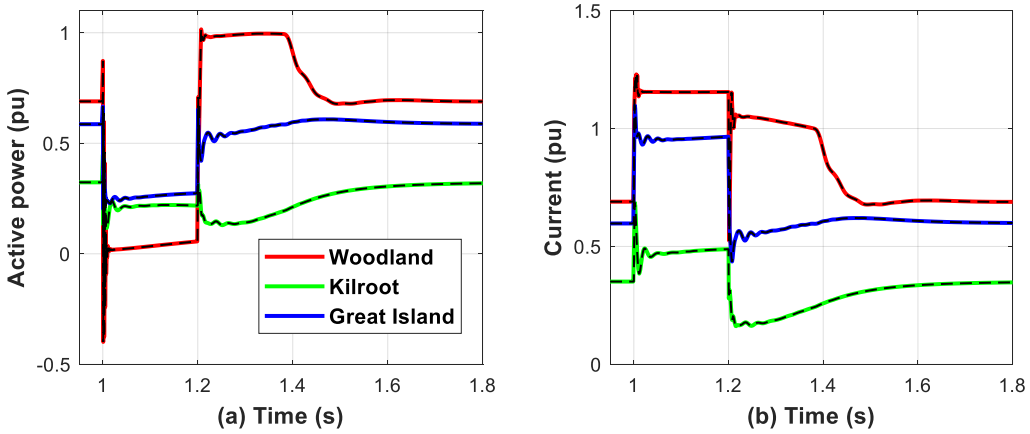

Figure 9.12: Active power output and injected current for three grid-forming inverters near Dublin, Belfast and Cork for a 200 ms, 3-phase bolted fault at the Woodland bus of the *Urban*

Irish grid with 100% grid-forming inverters under VSM control (droop control shown using dashed lines).

Finally, instead of all the grid-forming inverters adopting either a droop or dVOC control strategy, dVOC control is arbitrarily applied to the inverters at the Aghada, Great Island, Huntstown, Woodland, and Coolkeeragh buses, and also one of the inverters at Moneypoint and Ballylumford, while the remaining inverters employ droop control to create a "mixed" control strategy. For the same fault conditions and fault location as before, Figure 9.13 shows similar performance to Figures 9.8 and 9.10, indicating that the grid-forming control scheme chosen has minimal impact on the overall response. However, this conclusion assumes that each control strategy applies the same current limiting strategy, maximum current limit, and DC-side energy sources.

For the droop, dVOC and mixed control strategies, the system quickly recovers its initial state once the fault clears, with no/low oscillations observed during and post-fault. Similar results are achieved when the same fault is applied at all buses, which can be seen in [30]. It can be concluded that the system is robust for a grid-forming inverter only system.

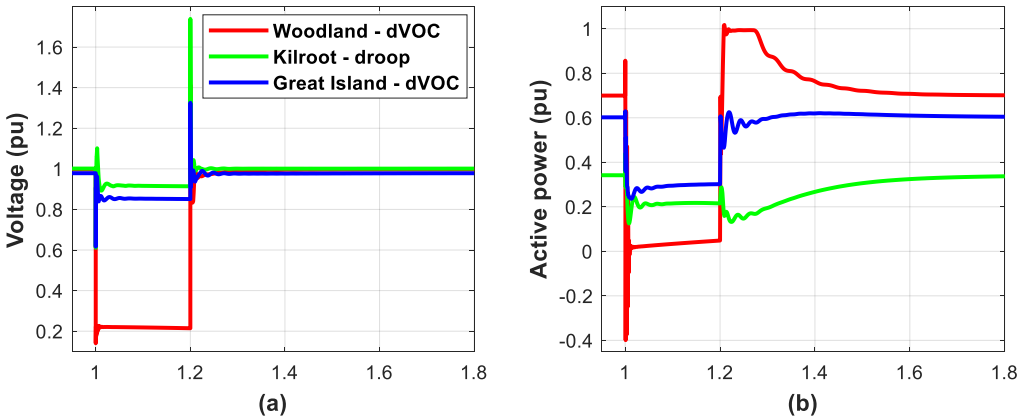

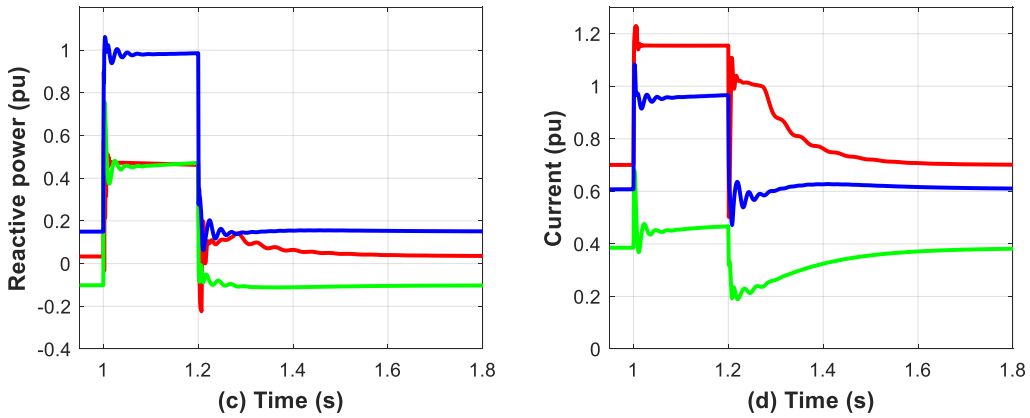

Figure 9.13: Voltage, active & reactive power output, and injected current for three grid-forming inverters near Dublin, Belfast and Cork for a 200 ms, 3-phase bolted fault at the Woodland bus of the *Urban* Irish grid with 100% grid-forming inverters for a mix of droop and dVOC controls (combination of VI and saturation current limiting controls applied).

9.3.3 *Remote* Irish grid with 100% GFMIs (current limiting strategies and virtual angular speed freezing)

Following on from the previous section, virtual impedance and (active and reactive current prioritised, scaled) current saturation current limiting with high/low limiting, with/without virtual angular speed freezing are now examined for the *Remote* grid, Figure 9.7(b).

9.3.3.1 Current saturation and virtual impedance limiting control

Case 1: 200 and 260 ms bolted 3-phase faults are applied at the Woodland bus in the *Remote* system, with droop based GFMIs under virtual impedance control and a current limit of 1.2 pu, *VI – 200 ms* and *VI – 260 ms*. Figure 9.14(d) shows that the "steady-state" injected current during the fault for the GFMI at Woodland remains within 1.2 pu, although the initial transient exceeds 1.4 pu. Compared to the GFMI at Woodland in Figure 9.8, Figure 9.14(a)-(c) shows that the GFMI under the *VI – 200 ms* scenario remains stable but takes longer to recover to its pre-fault state, indicating that the *Remote* system is less robust than the *Urban* configuration,

given that much of the generation is now located in the west while the major loads are still located in the east. Comparing the two fault durations for the *Remote* system, Figure 9.14 shows that the GFMI takes longer to recover for the longer fault, given that the virtual angle is continuously increasing during the fault.

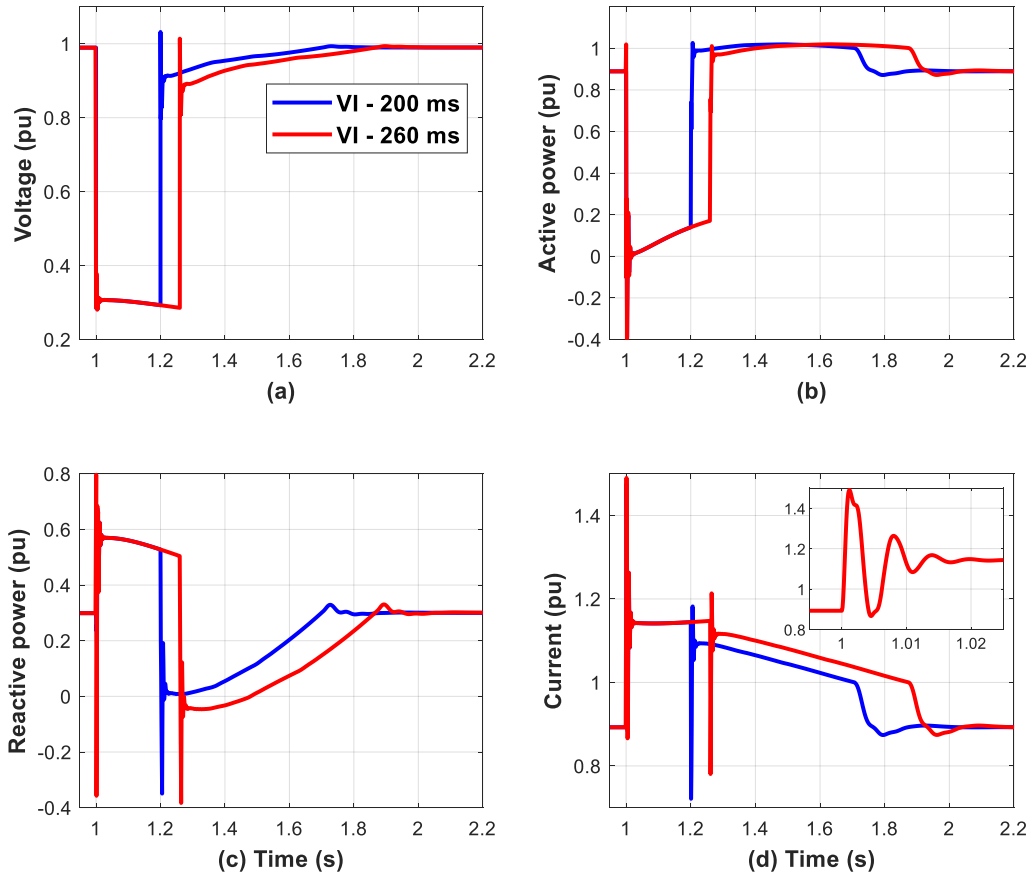

Figure 9.14: Voltage, active & reactive power output, and injected current for the grid-forming inverter at the Woodland bus for 200 and 260 ms, 3-phase bolted faults at the Woodland bus of the *Remote* Irish grid (Case 1), with 100% droop control grid-forming inverters incorporating virtual impedance control with $I_{max}^{VI} = 1.2$ pu.

Case 2: With the droop-based grid-forming inverters operating under current saturation control based on active, reactive current prioritisation or scaling, and the same current limit of 1.2 pu, a 260 ms, 3-phase bolted fault is applied at the Woodland bus, as in Case 1. Figure 9.15 shows the response of the inverter at Woodland, with the inverter current being strictly limited

within 1.2 pu under all three current reference saturation limiting approaches (initial current slightly exceeds 1.2 pu for ≈ 6 ms due to the one-step time delay (0.1 ms), implemented to represent signal measurement), Figure 9.15(d). Under reactive current priority, large oscillations are observed during the fault in the voltage, and active and reactive power output, for the grid-forming inverter. Under active current priority, the Woodland grid-forming inverter is unstable and doesn't return to its pre-fault state, since the injected current remains saturated after fault clearance, Figure 9.15(b). Active current prioritisation also leads to large voltage and power oscillations during and post fault clearance (see [43]), if the one-step time delay is removed (the time delay helps to smooth the inverter dynamics, and oscillations are largely avoided in Figure 9.15). In both scenarios, the high-frequency oscillations are excited by the LC filter, which is induced by the generated distorted d- and q-axis current references under active/reactive current prioritisation. Incorporating a resistor in series with the filter capacitor, C_f, helps to reduce the oscillations, but the frequency of the oscillations depends on the loading and system conditions, which makes it challenging to robustly design an appropriate filter. Furthermore, since active and reactive current prioritisation are not well aligned with the need to regulate both the active and reactive power, it follows that current saturation control based on active and reactive current prioritisation is not recommended for grid-forming inverters. Under the scaling strategy, Figure 9.15(a)-(c) shows that the inverter is unstable, but the high-frequency oscillations are not that severe, and the current returns to its pre-fault state ≈1.2 s after fault clearance, Figure 9.15(d), which confirms that current scaling can be combined with virtual impedance current limiting to strictly bound the grid-forming inverter current. In comparison to *VI – 260 ms* in Case 1, which is stable, the unstable scenarios in Case 2 indicate that virtual impedance control is more effective than current saturation limiting control in ensuring grid-forming inverter transient stability for faults.

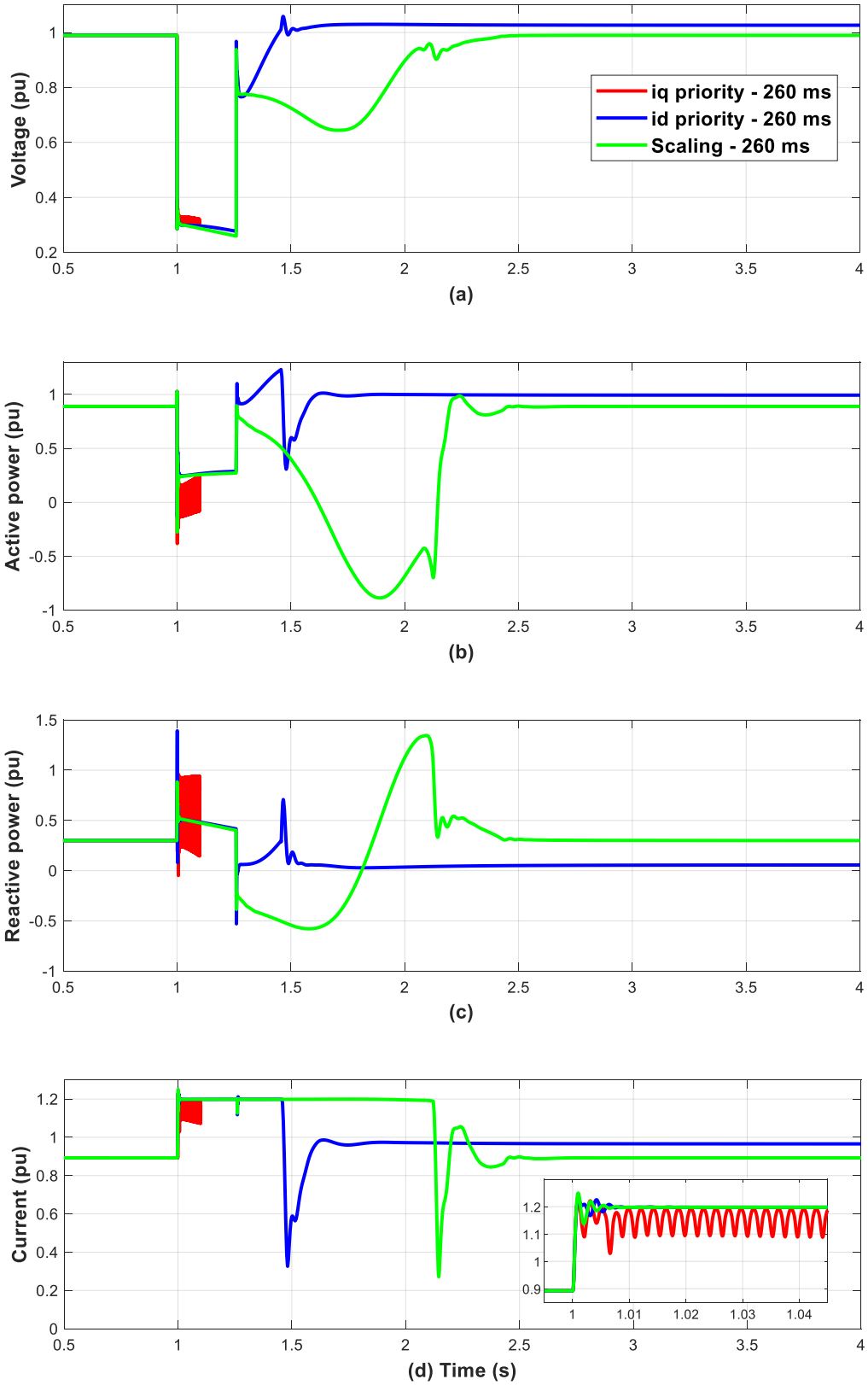

Figure 9.15: Voltage, active & reactive power output, and injected current for the grid-forming inverter at the Woodland bus for a 260 ms, 3-phase bolted fault at the Woodland bus of the

Remote Irish grid (Case 2), with grid-forming inverters applying active, reactive current priority, or scaling current saturation limiting with $I_{max} = 1.2$ pu.

Case 3: 3-phase faults are now considered at a different location, of a longer duration, and adopting an alternative current limiting approach for the grid-forming inverters, with $I_{max}^{VI} = I_{max} = 1.1$ pu, as follows: (1) 260 ms, 3-phase bolted fault at Aghada (near Cork) under VI control (*VI – 260 ms*); (2) same as (1) but for a 305 ms fault (*VI – 305 ms*); and (3) scaled current limits for a 200 ms fault (*Scaling – 200 ms*). Selecting $I_{max} = 1.1$ pu is intended to confirm that the *Remote* system is "weaker", as compared to Case 1 when $I_{max} = 1.2$ pu.

Voltage, current, active and reactive power are shown in Figure 9.16 for the grid-forming inverter at Aghada, the fault location. Unstable dynamics can be seen for *VI – 305 ms*, relative to the 260 ms fault duration scenario, while Figure 9.16(b) confirms that the inverter current is limited within 1.1 pu for both virtual impedance and current scaling, although the current is transiently higher with virtual impedance control (affecting converter lifetime). Figure 9.16(c)(d) shows that the grid-forming inverter is stable for the 260 ms fault, although it is comparatively slow (≈1.3 s) to recover. The inverter goes unstable for the 305 ms fault with VI control once the fault is cleared, since, for an extended period (> 1.8 s), the voltage and reactive power are low, and, at the same time, the active power falls highly negative (-1 pu), before returning to their pre-fault values. The instability is due to the extended acceleration of the inverter angular speed, with the regulation capability also lost, given that the injected current is at its limit. Later it will be seen that virtual angular speed freezing extends the grid-forming fault critical clearing time.

Current scaling also results in the inverter being unstable for a 200 ms fault, as the post-fault voltage is low and the active power falls highly negative, Figure 9.16(a)(b). Similar to Cases 1 and 2, the stable *VI – 260 ms* and unstable *Scaling – 200 ms* scenarios again indicate

that soft current limiting control leads to more robust grid-forming transient stability than hard saturation limiting.

Now considering the converter voltage, Figure 9.16(a) indicates that the voltage stays low for an extended period (> 1.3 s) for the two VI scenarios, while even for the stable *VI – 260 ms* scenario, voltage recovery is slow (≈ 1.3 s), suggesting that the fault critical clearing time at the Aghada location is close to 260 ms using VI current limit control. Comparing *VI – 260 ms* here ($I_{max}^{VI} = 1.1$ pu) against that in Case 1 ($I_{max}^{VI} = 1.2$ pu) indicates that the system takes longer to recover, noting the lower current limit.

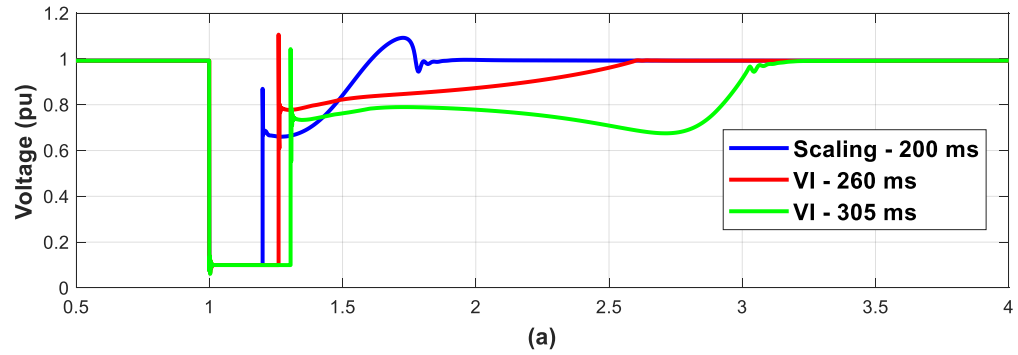

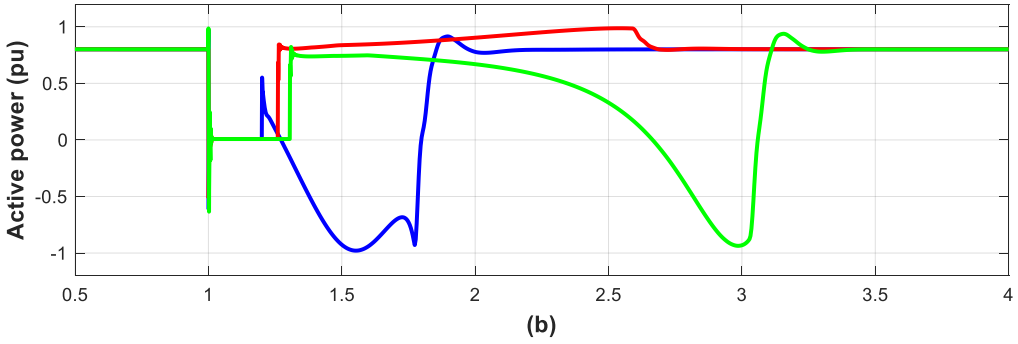

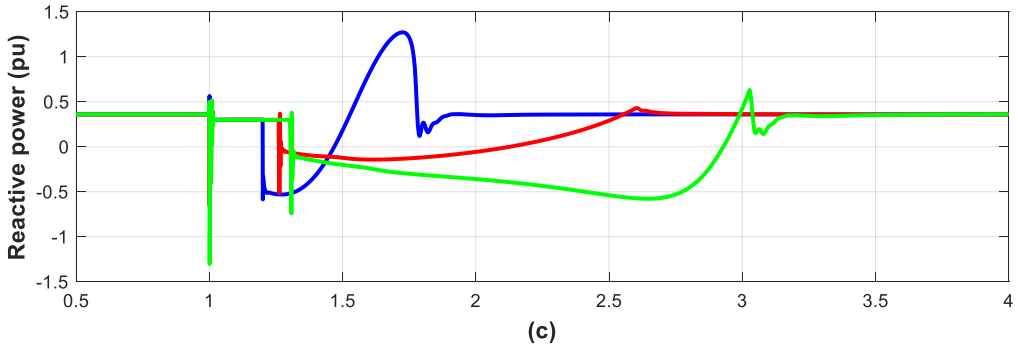

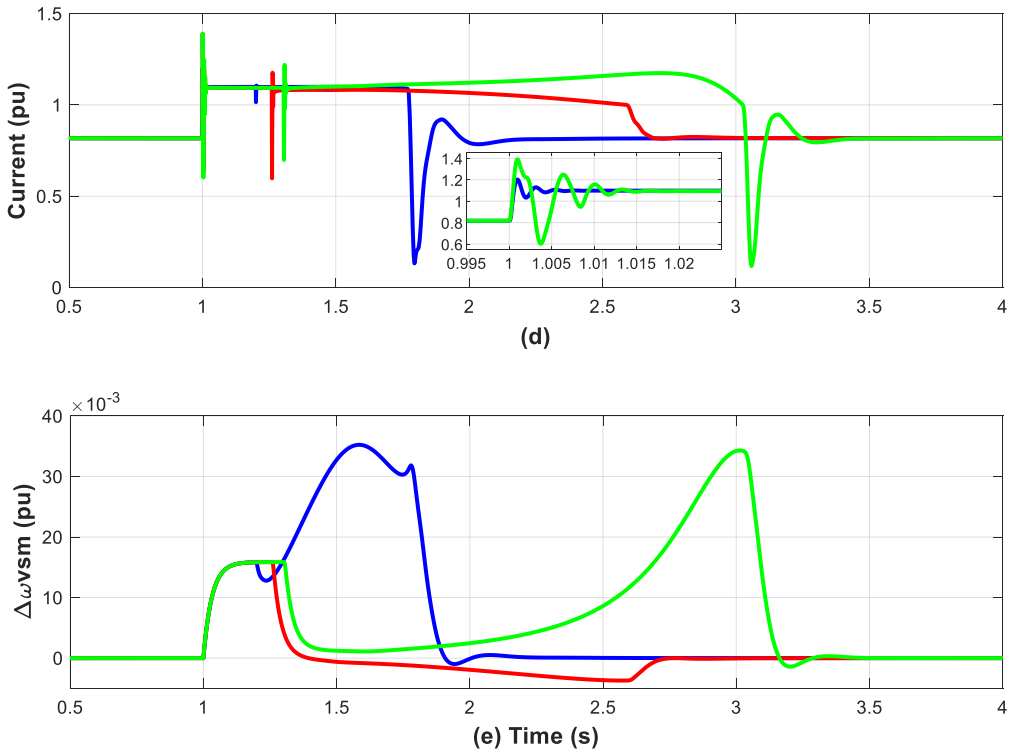

Figure 9.16: Impact of virtual impedance and scaling current reference saturation controls, and fault duration on the grid-forming transient stability at Aghada for 200, 260 and 305 ms 3-phase bolted faults at the Aghada bus for the *Remote* Irish grid with an overcurrent limit of 1.1 pu under Case 3.

9.3.3.2 GFMI transient stability enhanced by virtual angular speed freezing

Case 4: Previously in Cases 1 - 3, virtual impedance control was seen to be the preferred option, but stability was affected for faults longer than ≈260 ms. Freezing of the virtual angular speed (Equation 9.10) is now introduced for the same fault conditions as Case 3: (1) virtual impedance control combined with virtual angular speed freezing for a 505 ms, 3-phase bolted fault at Aghada (*VI + Frozen – 505 ms*); (2) *Scaling + Frozen – 505 ms*; and (3) both current limiting control approaches for a 600 ms fault (*Hybrid + Freeze – 600 ms*). In order to achieve a fair comparison with Case 3, the current limiting values I_{max}^{VI}, I_{max} for (1) and (2) are unchanged at 1.1 pu, and for (3), 1.1 and 1.15 pu respectively for VI and scaling.

Results for the grid-forming inverter at Aghada are shown in Figure 9.17, and, as previously, the "steady-state" current is limited within 1.1 pu for both the virtual impedance and current scaling approaches, Figure 9.17(d). The initial post-fault voltage for *VI + Frozen – 505 ms*, Figure 9.17(a), is close to the pre-fault value, and, significantly, 0.2 pu higher when compared against *VI – 260 ms*, Figure 9.16(a). The voltage and active power also recover much more quickly (≈0.1 s to reach the pre-fault state, relative to ≈1.3 s). It can be seen in Figure 9.17(c) that freezing the virtual angular speed increases the critical clearing time for the *VI*, *Scaling* and *Hybrid* approaches, with inverter stability maintained, even for 600 ms faults. Figure 9.17(b) shows that compared to the other VI scenarios, the scaling approach results in slightly lower post-fault active power, but the inverter quickly recovers to its pre-fault state. In conclusion, freezing the virtual angular speed improves the transient stability of the grid-forming inverter, irrespective of the current limiting strategy, with an improved post-fault initial voltage, a faster post-fault recovery, and an extended fault ride through capability.

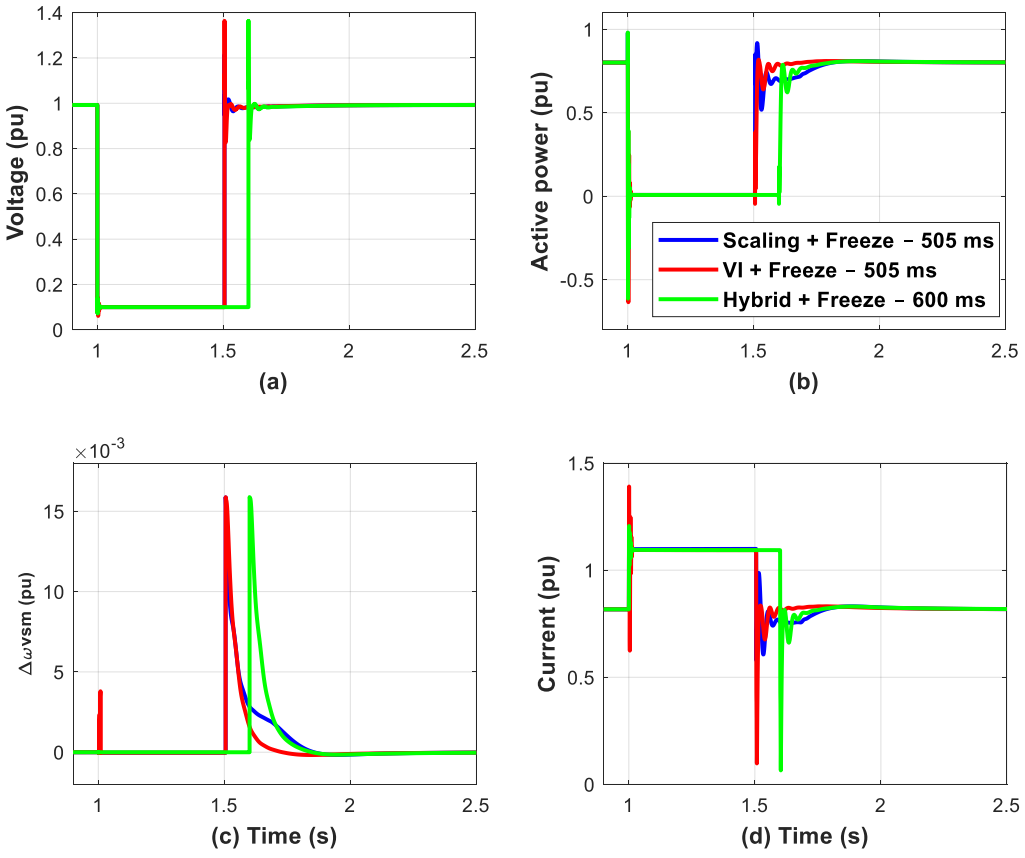

Figure 9.17: Impact of virtual impedance and scaling current reference saturation controls, and freezing of virtual angular speed on the grid-forming inverter at Aghada for 505 and 600 ms 3-phase bolted faults at the Aghada bus of the *Remote* Irish grid with an overcurrent limit of 1.1 pu (Case 4).

9.4 Conclusions

The transient stability of a power system containing a high share of grid-forming inverters can be significantly different to that of a traditional synchronous generator-based system, recognising the lower capacity (current) headroom, but flexible control capability, of power electronic inverters. System stability was investigated for a future Irish grid consisting entirely of grid-forming inverters under three-phase fault conditions with the inverters placed at existing locations for large-scale conventional generation. Electromagnetic transient (EMT) simulations showed that a 100% grid-forming inverter system, employing either droop control (or virtual synchronous machine), dispatchable virtual oscillator control, or a mix of both, under a combination of VI and scaling current saturation limiting control, was robust against 3-phase faults, with consistent performance being achieved, despite variations in fault location or inverter control methods.

A modified grid configuration was also investigated, with the inverters being placed at more remote locations, recognising likely locations for wind farms. Simulation results show that the *Remote* system is weaker than the above *Urban* system. For a reduced overcurrent limit, the grid-forming inverters typically took more than 1 s to recover to their pre-fault state under virtual impedance current limiting control, when 260 ms, 3-phase faults were applied, and they could go unstable with the current scaling saturation approach for a 200 ms fault. However, by freezing the virtual angular speed during the fault, for both the virtual impedance and current scaling approaches, the grid-forming inverters remained stable, even with a reduced

current limit, and the pre-fault state was quickly recovered, even for 600 ms faults, indicating an increased fault critical clearing time. Time domain simulations also show that when active or reactive current prioritisation current saturation controls are applied that grid-forming inverters can introduce large, high-frequency resonance oscillations, but a scaling-down current saturation approach can help to mitigate such problems by generating smoother current references.

References

[1] RTE, "Description of system needs and test cases," MIGRATE WP3, 2016. Available: https://www.h2020-migrate.eu/downloads.html. [Accessed: 27/5/21]

[2] Hodge, B.-M., Jain, H., Brancucci, C., et al., "Addressing technical challenges in 100% variable inverter-based renewable energy power systems," *Wiley Interdiscip. Rev. Energy Environ.*, 2020, 9, (5), e376.

[3] IEEE PES, "Stability definitions and characterization of dynamic behavior in systems with high penetration of power electronic interfaced technologies," Tech. Rep. PES-TR77, May 2020.

[4] Holttinen, H., Kiviluoma, J., Flynn, D., et al., "System impact studies for near 100% renewable energy systems dominated by inverter based variable generation," *IEEE Trans. Power Syst.*, 37(4), pp. 3249-3258, 2022.

[5] Zhao, X., and Flynn, D., "Transient stability enhancement with high shares of grid-following converters in a 100% converter grid," in *IEEE PES Innovative Smart Grid Technologies Europe (ISGT-Europe)*, pp. 594-598, Oct. 2020.

[6] Matevosyan, J., Badrzadeh, B., Prevost, T., et al., "Grid-forming inverters: are they the key for high renewable penetration?," *IEEE Power Energy Mag.*, 17, (6), pp. 89-98, 2019.

[7] Chandorkar, M.C., Divan, D.M. and Adapa, R., "Control of parallel connected inverters in standalone AC supply systems," *IEEE Trans. Ind. Appl.*, 29(1), pp. 136-143, 1993.

[8] Zhang, L., Harnefors, L. and Nee, H.P., "Power-synchronization control of grid-connected voltage-source converters," *IEEE Trans. Power Syst.*, 25(2), pp. 809-820, 2010.

[9] Simpson-Porco, J.W., Dörfler, F. and Bullo, F., "Synchronization and power sharing for droop-controlled inverters in islanded microgrids," *Automatica*, 49(9), pp. 2603-2611, 2013.

[10] Zhong, Q.C. and Weiss, G., "Synchronverters: inverters that mimic synchronous generators," *IEEE Trans. Ind. Electron.*, 58(4), pp. 1259-1267, 2010.

[11] D'Arco, S., Suul, J.A. and Fosso, O.B., "A virtual synchronous machine implementation for distributed control of power converters in smart grids," *Electr. Power Syst. Res.*, 122, pp. 180–197, 2015.

[12] Guan, M., Pan, W., Zhang, J., et al., "Synchronous generator emulation control strategy for voltage source converter (VSC) stations," *IEEE Trans Power Syst.*, 30(6), pp. 3093-3101, 2015.

[13] Cvetkovic, I., Boroyevich, D., Burgos, et al., "Modeling and control of grid-connected voltage-source converters emulating isotropic and anisotropic synchronous machines," in *IEEE Workshop on Control Model. Power Electron. (COMPEL)*, 2015.

[14] Arghir, C., Jouini, T. and Dörfler, F., "Grid-forming control for power converters based

on matching of synchronous machines," *Automatica*, 95, pp. 273-282, 2018.

[15] Huang, L., Xin, H., Wang, Z., et al., "A virtual synchronous control for voltage-source converters utilizing dynamics of DC-link capacitor to realize self-synchronization," *IEEE J. Emerg. Sel. Topics Power Electron.*, 5(4), pp. 1565-1577, 2017.

[16] B. Johnson, M. Sinha, N. Ainsworth, et al., "Synthesizing virtual oscillators to control islanded inverters," *IEEE Trans. Power Electron.*, 31(8), pp. 6002–6015, 2015.

[17] Seo, G.-S., Colombino, M., Subotic, I., et al., "Dispatchable virtual oscillator control for decentralized inverter-dominated power systems: analysis and experiments," in *IEEE Appl. Power Electron. Conf. Expo.*, pp. 561-566, 2019.

[18] Musca, R., Vasile, A. and Zizzo, G., "Grid-forming converters. a critical review of pilot projects and demonstrators," *Renew. Sust. Energ. Rev.*, 165, 112551, 2022.

[19] Gevorgian, V., Shah, S., Yan, W., et al., "Grid-forming wind power," ESIG Spring Technical Workshop Tucson, AZ, March 22, 2022. https://www.nrel.gov/docs/fy22osti/82509.pdf

[20] Milano, F., Dörfler, F., Hug, et al., "Foundations and challenges of low-inertia systems," in *Proc. Power Syst. Comput. Conf.*, Ireland, 2018.

[21] Sadeghkhani, I., Golshan, M.E.H., Guerrero, et al., "A current limiting strategy to improve fault ride-through of inverter interfaced autonomous microgrids," *IEEE Trans. Smart Grid*, 8(5), pp. 2138-2148, 2016.

[22] Huang, L., Xin, H., Wang, et al., "Transient stability analysis and control design of droop-controlled voltage source converters considering current limitation," *IEEE Trans. Smart Grid*, 10(1), pp. 578-591, 2017.

[23] Taul, M.G., Wang, X., Davari, P. et al., "Current limiting control with enhanced dynamics of grid-forming converters during fault conditions," *IEEE J. Emerg. Sel. Topics Power Electron.*, 8(2), pp. 1062-1073, 2019.

[24] Paquette, A. D., and Divan, D. M., "Virtual impedance current limiting for inverters in microgrids with synchronous generators," *IEEE Trans. Ind. Appl.*, 51(2), pp. 1630-1638, 2014.

[25] Groß, D. and Dörfler, F., "Projected grid-forming control for current-limiting of power converters," In *Allerton Conference on Communication, Control, and Computing*, pp. 326-333, 2019.

[26] Zhao, X. and Flynn, D., "Freezing grid-forming converter virtual angular speed to enhance transient stability under current reference limiting," in *IEEE 21st Workshop on Control and Modeling for Power Electronics (COMPEL 2020)*, 2020.

[27] Zhao, X. and Flynn, D., "Grid-forming converter current limiting design to enhance transient stability for grid phase jump events," in *11th IFAC Symposium on Control of Power and Energy Systems (CPES)*, 2022.

[28] Poolla, B.K., Groß, D. and Dörfler, F., "Placement and implementation of grid-forming

and grid-following virtual inertia and fast frequency response," *IEEE Trans. Power Syst.*, 34(4), pp. 3035-3046, 2019.

[29] Yang, C., Huang, L., Xin, H. et al, "Placing grid-forming converters to enhance small signal stability of PLL-integrated power systems," *IEEE Trans. Power Syst.*, 36(4), pp. 3563-3573, 2020.

[30] Thakurta, P., Zhao, X., Flynn, D., "Local Control and Simulation Tools for Large Transmission Systems," EU H2020 MIGRATE WP3, 2019.

[31] Zhao, X., Thakurta, P.G. and Flynn, D., "Grid-forming requirements based on stability assessment for 100% converter-based Irish power system," *IET Renew. Power Gener.*, 16(3), pp. 447-458, 2022.

[32] Qoria, T., Cossart, Q., Li, C., Guillaud, et al., "Deliverable 3.2: Local control and simulation tools for large transmission systems," *MIGRATE project*, 2018.

[33] Zhao, X. and Flynn, D., "Stability enhancement strategies for a 100% grid-forming and grid-following converter-based Irish power system," *IET Renew. Power Gener.*, 16(1), pp. 125-138, 2022.

[34] Rokrok, E., Qoria, T., Bruyere, et al., "Transient stability assessment and enhancement of grid-forming converters embedding current reference saturation as current limiting strategy," *IEEE Trans. Power Syst.*, 2021. DOI: 10.1109/TPWRS.2021.3107959.

[35] Groß, D., Colombino, M., Brouillon, J.-S., et al., "The effect of transmission-line dynamics on grid-forming dispatchable virtual oscillator control," *IEEE Trans. Contr. Netw. Syst.*, 6, (3), pp. 1148-1160, 2019.

[36] Seo, G.S., Colombino, M., Subotic, I., et al., "Dispatchable virtual oscillator control for decentralized inverter-dominated power systems: Analysis and experiments," in *Proc. IEEE Appl. Power Electron. Conf. Expo. (APEC)*, March 2019.

[37] Dymola Systems Engineering, https://www.3ds.com/products-services/catia/products/dymola/

[38] Zhao, X. and Flynn, D., "Grid-forming converter angular speed freezing to enhance transient stability in 100% grid-forming and mixed power systems", in *11th IFAC Symposium on Control of Power and Energy Systems (CPES)*, 2022.

[39] EirGrid, "All-Island ten year transmission forecast statement 2020," 2020.

[40] EirGrid and SONI, "Shaping our electricity future," Technical Report, March 2021.

[41] EirGrid and SONI, "Operational Constraints Update 28/06/2021," Jun. 2021.

[42] EirGrid, "Tomorrow's Energy Scenarios Consultation Ireland - Planning our Energy Future," 2019.

[43] Zhao, X. and Flynn, D., "Stability enhancement strategies for a 100% grid-forming and grid-following converter-based Irish power system," *IET Renew. Power Gener.*, 16(1), pp. 125-138, 2022.